Research Article

Dose-dependent immunomodulatory effects of silver-doped nanostructured bioglasses in calvarial bone repair

Gustavo Henrique Marques Ribeiro[1†], Rafael Obata Trevisan[1†], Malu Mateus Santo Obata[1], Chamberttan S. Desidério[2], Odival Seabra[1], Renata Margarida Etchebehere[3], Carlo José Freire Oliveira[2], Noelio Oliveira Dantas[4], Anielle Christine Almeida Silva[5], Hugo F. Perini[2], Marcos Vinicius da Silva[2], Sanívia Aparecida de Lima Pereira[6,7], and Rodrigo César Rosa[1*]

[1]Department of Structural Biology, Institute of Biological and Natural Sciences, Federal University of Triângulo Mineiro, Uberaba, Minas Gerais 38025-350, Brazil
[2]Department of Microbiology, Immunology and Parasitology, Institute of Biological and Natural Sciences, Federal University of Triângulo Mineiro, Uberaba, Minas Gerais 38025-350, Brazil
[3]Department of Surgical Clinic, Institute of Health Sciences, Federal University of Triângulo Mineiro, Uberaba, Minas Gerais 38025-350, Brazil
[4]Department of Physical Sciences, Physics Institute, Federal University of Alagoas, Maceió, Alagoas 57072-900, Brazil
[5]Department of Physical Sciences, Physics Institute, Federal University of Uberlândia, Uberlândia, Minas Gerais 38025-350, Brazil
[6]Postgraduate Program in Dentistry, University of Uberaba, Uberaba, Minas Gerais 38055-500, Brazil
[7]Center for Professional Education, Federal University of Triângulo Mineiro, Uberaba, Minas Gerais 38025-350, Brazil
[†]*These authors contributed equally to this work.*

Abstract

Background: Silver-doped nanostructured bioglasses have emerged as promising biomaterials for bone repair due to their bioactivity and potential to modulate immune–inflammatory responses. **Objective**: To assess immune–inflammatory modulation by silver-doped nanostructured bioglasses during bone repair in rat calvarial defects. **Methods**: In this study, nanostructured bioglasses were synthesized using a melt-quench method with silicon dioxide, sodium carbonate, calcium carbonate, and phosphorus pentoxide as precursors, followed by the incorporation of silver(I) oxide at concentrations ranging from 0.25 to 1.50 wt%. **Results**: Structural characterization confirmed the amorphous nature of the materials and the homogeneous incorporation of silver (Ag), forming nanoscale features at the bioglass surface. Eighty male Wistar rats were subjected to critical-size calvarial defect surgery to evaluate tissue response, inflammatory modulation, and systemic safety after bioglass implantation. Histological analysis demonstrated limited residual material particles and predominantly mild inflammatory infiltrates across treated groups, while hepatic and renal tissues exhibited preserved histoarchitecture, confirming the absence of systemic toxicity. Systemic cytokine profiling revealed a concentration-dependent immunomodulatory effect. Pure bioglass (Ag-0.00) and high silver content (Ag-1.50) enhanced the production of anti-inflammatory cytokines interleukin-4 and interleukin-10, whereas intermediate Ag concentrations (Ag-0.50–0.75) selectively increased pro-inflammatory mediators, including tumor

***Corresponding author:**
Rodrigo César Rosa (rodrigo.rosa@uftm.edu.br)

Submitted: 07 October 2025; Revision received: 12 December 2025; Accepted: 22 December 2025; Published: 03 March 2026

How to cite this article: Ribeiro GHM, Trevisan RO, Obata MMS, *et al*. Dose-dependent immunomodulatory effects of silver-doped nanostructured bioglasses in calvarial bone repair. *J Biol Methods*. 2026;13(1):e99010098. DOI: 10.14440/jbm.0323

necrosis factor alpha and interferon gamma. These patterns suggest that Ag content influences the balance between immune activation and resolution phases during bone repair. Intermediate concentrations were associated with improved tissue organization and histological features compatible with early reparative processes, whereas higher concentrations favored a regulatory inflammatory profile compatible with later stages of healing. **Conclusion**: Overall, the findings demonstrate that Ag incorporation enables fine-tuned, dose-dependent modulation of immune–inflammatory responses while maintaining systemic biocompatibility, supporting the potential of Ag-doped nanostructured bioglasses as multifunctional candidates for bone repair applications.

Keywords: Immunomodulation, Osteoimmunology, Bioglass, Silver nanoparticles, Bone repair

1. Introduction

Bone regeneration remains a major clinical challenge, particularly in conditions associated with trauma, infection, tumor resection, or congenital defects. Effective bone healing depends on a tightly coordinated sequence of inflammatory, cellular, and remodeling events that are critically regulated by both innate and adaptive immune responses. Immediately after injury or biomaterial implantation, neutrophils and monocytes/macrophages are rapidly recruited to the defect site, where they participate in debris clearance and initiate early molecular signaling. Although this acute inflammatory phase is essential for repair, excessive or prolonged inflammation can impair angiogenesis, osteoblast differentiation, and extracellular matrix deposition, ultimately compromising regenerative processes.[1-3]

Advances in osteoimmunology have demonstrated that bone repair relies on a finely regulated immune environment characterized by the dynamic interplay between pro-inflammatory mediators, such as interleukin (IL)-6, tumor necrosis factor alpha (TNF-α), and interferon gamma (IFN-γ), and regulatory cytokines, including IL-4 and IL-10. Disruption of this balance may lead to persistent inflammation and altered tissue remodeling. An updated overview of these immunological mechanisms in orthopedic and regenerative contexts has been provided by Moldovan *et al*.,[4] underscoring the importance of immune profiling in bone repair studies.

Despite significant advances in regenerative strategies, effective bone repair remains particularly challenging in scenarios involving extensive bone loss or disruption of the extracellular matrix. In such conditions, bone substitutes are required to provide temporary structural support while being progressively resorbed and replaced by newly formed bone.[5-8] The success of this process depends not only on the intrinsic bioactivity of the material but also on its capacity to elicit a controlled host response. Upon implantation, biomaterials inevitably interact with the immune system, triggering nonspecific cellular responses that may support or impair tissue repair.[9] Although numerous organic and synthetic bone substitutes have been developed, none fully satisfy the criteria required for predictable and reproducible bone regeneration, highlighting the need for experimental approaches capable of systematically assessing host–material immune interactions.[3,10]

Within this context, bioglasses have emerged as widely used platforms in bone regeneration research due to their bioactivity, ability to form a hydroxycarbonate apatite layer, controlled ionic dissolution, and compatibility with bone-forming cells.[3,7] Their performance as bone substitutes is strongly influenced by the immune environment, reinforcing the relevance of immune-focused analytical frameworks when evaluating these materials.[6,10]

Nanostructured bioglasses represent a significant technological advancement, as nanoscale features enhance surface reactivity, dissolution kinetics, and interactions with immune and progenitor cells. These properties make nanostructured systems particularly suitable for investigating immune-mediated mechanisms associated with bone repair and biomaterial integration.[11-15] Accordingly, osteoimmunomodulation has become a central concept in the evaluation of regenerative biomaterials, emphasizing the need for experimental strategies that integrate immune readouts into material assessment.[13-15]

The incorporation of metallic ions, particularly silver (Ag), has been widely explored to modify the biological behavior of bioglasses. While Ag is traditionally investigated for its antimicrobial and physicochemical properties, accumulating evidence indicates that it can also influence immune signaling in a concentration-dependent manner.[14,16] However, most studies have focused on limited Ag concentrations or have prioritized material characterization, with comparatively less emphasis on standardized approaches to assess systemic and local immune–inflammatory responses across a defined dose range.

To address this methodological gap, the present study describes a reproducible experimental framework to evaluate systemic and local immune–inflammatory responses elicited by nanostructured bioglasses doped with increasing Ag concentrations (0.00–1.50 wt%) using a rat calvarial critical-size defect model. The central premise of this work is that a dose-resolved experimental design enables

systematic assessment of how variations in Ag content are reflected in distinct immune–inflammatory readouts, without presupposing specific mechanistic pathways. Regulatory and pro-inflammatory cytokines were therefore selected as standardized indicators to capture these responses within the proposed framework.

2. Materials and methods

2.1. Synthesis and characterization

Nanostructured bioglasses belonging to the silicon dioxide–sodium oxide–calcium oxide–phosphorus pentoxide vitreous system were synthesized using the melting method. Analytical-grade precursors—silicon dioxide (30–60 wt%), sodium carbonate (10–40 wt%), calcium carbonate (10–40 wt%), and phosphorus pentoxide (1–10 wt%) were homogenized and subjected to controlled thermal treatment between 1,000 and 2,000 °C. This process ensured adequate mixing and structural stability of the resulting bioglass. The nanostructured variants were doped by adding Ag oxide to achieve Ag contents of 0.25–1.5 wt%, following a procedure described in a patent application (INPI: BR 10 2025 003053 5).

The materials underwent structural and morphological characterization to confirm their amorphous nature and evaluate the possibility of crystalline phase formation. X-ray diffraction analyses were performed using a Bruker (United States) D8 Focus diffractometer with a copper anode and monochromator, covering an angular range of 20° to 60° (2θ) at a scanning speed of 2°/minute, all at room temperature. Complementary optical absorption spectroscopy was performed at ambient conditions using a Shimadzu (Japan) ultraviolet–visible–near-infrared 3600 spectrometer, with a spectral resolution of 1 nm, to assess the electronic transitions and optical responses of the synthesized samples. Additionally, surface topography and particle morphology were examined using atomic force microscopy (AFM) with a Shimadzu (Japan) SPM 9700 system. Both dynamic and phase modes were employed with NT-MDT cantilevers, and the acquired data were processed using the Gwyddion software (version 2.63), enabling the generation of two- and three-dimensional images and surface profile analyses.

2.2. Animals and experimental design

All experimental procedures were conducted in accordance with the Guide for the Care and Use of Laboratory Animals (National Institutes of Health) and approved by the Institutional Animal Care and Use Committee (CEUA/UNIUBE, protocol no. 004/2021).

A total of 80 male Wistar albino rats (*Rattus norvegicus*) (Animal Facility of the Federal University of Uberlândia (UFU), Brazil), weighing 140–160 g, were housed in standard polypropylene cages under controlled environmental conditions (22 ± 2 °C, 55 ± 5% relative humidity, 12 hours light/dark cycle). Animals had free access to water and a commercial diet (Nuvilab CR-1, Brazil).

Critical-size calvarial bone defects were surgically created in the right parietal bone, lateral to the sagittal suture, using a 4 mm trephine bur coupled to a contra-angle handpiece (20,000 rpm) under continuous sterile saline irrigation. The defect depth was standardized at 1.5 mm, with special care to avoid damage to the underlying dura mater. All procedures were performed under sterile conditions, and representative images of defect creation and material placement are shown in Figure 1.

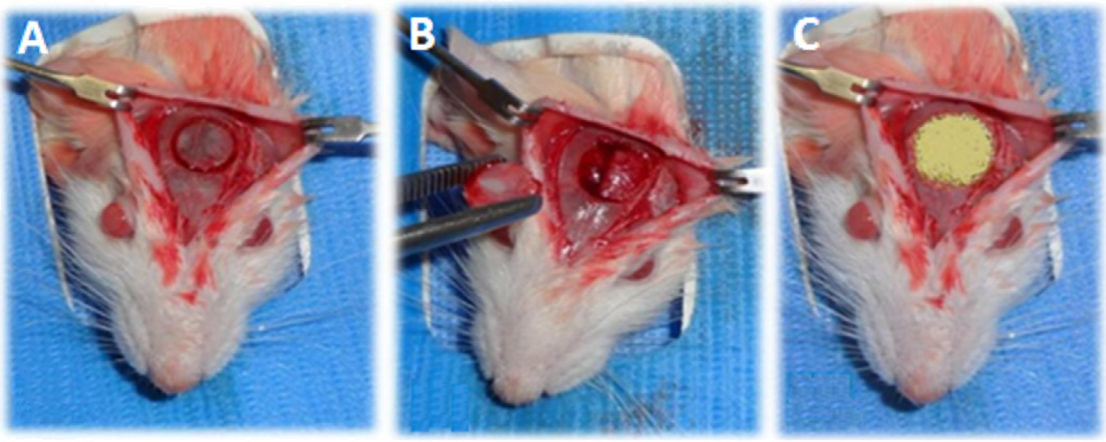

Figure 1. Surgical procedure for the rat calvarial critical-size defect model. (A) Exposure of the parietal bone following skin incision and periosteal reflection, showing the standardized circular critical-size defect immediately after drilling with a trephine bur under constant saline irrigation. (B) Image taken immediately after defect preparation. (C) Critical-size calvarial bone defect filled with silver-doped nanostructured bioglass.

Animals were randomly allocated into eight experimental groups (n = 10 per group): (i) control (C): defect filled with blood clot only; (ii) Ag-0.00 (pure bioglass): defect filled with undoped bioglass; (iii) Ag-doped bioglasses: defects filled with nanostructured bioglass doped with Ag oxide at 0.25, 0.50, 0.75, 1.00, 1.25, or 1.50 wt%.

The sample size was defined a priori based on precedent in the literature, using rat calvarial critical-size defect models for biomaterial evaluation. Similar studies commonly employ group sizes of 8–10 animals to enable histopathological and immunological analyses while adhering to ethical principles for animal experimentation. Accordingly, a group of 10 animals per experimental condition was selected, consistent with previously reported designs.[17]

At four weeks postoperatively, animals were euthanized via intraperitoneal injection of xylazine hydrochloride (50 mg/kg), following humane endpoints and ethical standards.

2.3. Histopathological and immunological evaluation

After euthanasia, calvarial specimens were collected, fixed in 10% neutral buffered formalin, decalcified in 10% ethylenediaminetetraacetic acid, and processed for paraffin embedding. Serial sections (5 µm) were stained with hematoxylin–eosin and examined under light microscopy (Olympus BX41®, Olympus, Japan). The presence of residual bioglass crystals and the degree of inflammatory cell infiltration were assessed semi-quantitatively by three blinded observers, both within the defect area and at its periphery. The scoring criteria were: 0 = absent, 1 = mild, 2 = moderate, and 3 = intense. For statistical analysis, scores 0 and 1 were pooled (mild/absent), and scores 2 and 3 were pooled (moderate/intense).

To assess potential systemic toxicity, histopathological examinations were also performed on liver and kidney tissues collected immediately after euthanasia. Hepatic evaluation included inflammatory cell infiltration, hydropic degeneration, cellular swelling, sinusoidal dilation, vascular congestion, perivascular infiltrate, and necrosis. Renal evaluation included alterations in filtration space (increased or reduced), cortical and medullary cell swelling, vascular congestion, cytoplasmic vacuolization, inflammatory cell infiltration, tubular dilatation, hyaline material deposition, and necrosis. All parameters were graded according to a semi-quantitative scale of intensity (0 = absent, 1 = mild, 2 = moderate, 3 = severe). Data are summarized in descriptive tables (Tables 1 and 2) for comparison between the C and the bioglass groups.

In parallel, systemic immune modulation was investigated by quantifying plasma cytokines. Blood was collected via cardiac puncture into heparinized tubes, centrifuged at 3,000 rpm for 10 min, and plasma samples were stored at −80 °C until analysis. Cytokine concentrations (IL-4, IL-10, IL-6, TNF-α, and IFN-γ) were determined using enzyme-linked immunosorbent assay (ELISA; BD Biosciences, United States), according to the manufacturer's instructions, and expressed in pg/mL.

2.4. Statistical analysis

Data were analyzed using GraphPad Prism 8.1. Normality was assessed using the D'Agostino–Pearson test. Non-parametric data were analyzed using the Mann–Whitney test or Kruskal–Wallis with Dunn's post hoc test. Parametric data were analyzed using one-way analysis of variance with Tukey's post hoc test. Statistical significance was set at $p < 0.05$.

Table 1. Histological scores of hepatic tissue in control and bioglass-treated rats after four weeks

Parameter	Control group (n = 10)				Bioglass-treated group (n = 10)			
	0	1	2	3	0	1	2	3
Presence of inflammatory cells	1	7	1	0	2	8	0	0
Hydropic degeneration	7	3	0	0	7	1	2	0
Cellular swelling	7	3	0	0	8	1	1	0
Sinusoidal dilation	9	1	0	0	9	1	0	0
Vascular congestion	8	1	0	0	7	1	1	0
Perivascular infiltration	6	3	1	0	7	1	2	0
Necrosis	7	3	0	0	8	1	1	0

Note: 0 = absent; 1 = mild; 2 = moderate; 3 = severe. Bioglass-treated group refers to the group treated with pure bioglass.

3. Results

3.1. Characterization of nanostructured bioglass

X-ray diffraction analysis confirmed the amorphous nature of the synthesized bioglass, as evidenced by the presence of broad diffraction bands without detectable crystalline phases. A characteristic peak was observed between 22° and 30°, consistent with the presence of vitreous materials. The full-width at half maximum analysis supported the nanostructured profile of the material, and progressive Ag incorporation resulted in a slight decrease in peak intensity, possibly reflecting increased structural disorder or the formation of nanoscale Ag clusters without distinct diffraction peaks (Figure 2).

Optical absorption spectra revealed an intrinsic absorption band around 240 nm, associated with the bioglass matrix, and a broad localized surface plasmon resonance peak between

Table 2. Histological scores of renal tissue in control and bioglass-treated rats after four weeks

Parameter	Control group (n = 10)				Bioglass-treated group (n = 10)			
	0	1	2	3	0	1	2	3
Increased filtration space	9	1	0	0	10	0	0	0
Reduced filtration space	8	1	1	0	9	1	0	0
Cortical cellular swelling	8	2	0	0	8	1	1	0
Medullary cellular swelling	8	1	1	0	9	2	0	0
Cortical vascular congestion	9	1	0	0	7	2	1	0
Cytoplasmic vacuolization	7	2	1	0	8	2	0	0
Infiltration of inflammatory cells	10	0	0	0	9	1	0	0
Distal convoluted tubule dilation	10	0	0	0	9	1	0	0
Deposition of hyaline material	1	7	2	0	2	6	2	0
Necrosis	2	7	1	0	1	8	1	0

Notes: 0 = absent; 1 = mild; 2 = moderate; 3 = severe. Bioglass-treated group refers to the group treated with pure bioglass.

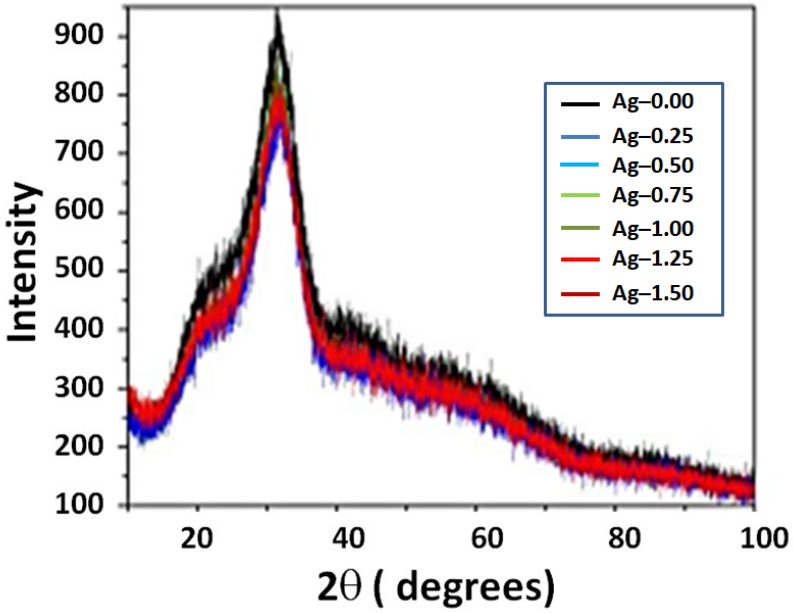

Figure 2. X-ray diffraction patterns of pure and silver (Ag)-doped (0.25–1.5 wt% Ag) nanostructured bioglasses. These analyses confirm the amorphous nature and homogeneous incorporation of Ag in all compositions.

360 and 420 nm, confirming the presence of Ag nanoparticles (AgNPs) within the matrix. The localized surface plasmon resonance peak intensity increased proportionally to Ag content, while slight spectral shifts suggested changes in nanoparticle size and distribution. Absorbance beyond 500 nm remained low, indicating homogeneous dispersion without significant aggregation (Figure 3).

Atomic force microscopy was employed to characterize the nanostructured bioglass and assess the distribution of AgNPs within its structure. Figure 4A presents the AFM phase image, where distinct contrast variations were observed, confirming the localization of nanoparticles along the material surface. The heterogeneous contrast suggests differences in composition, adhesion, or viscoelastic properties, while the sharply defined central region surrounded by fragmented structures indicates localized deposition or degradation processes relevant to the interaction of bioglass with biological environments.

The three-dimensional topography of an individual nanostructure (Figure 4B) highlights protrusions with lateral dimensions of approximately 1 µm, consistent with the presence of AgNP agglomerates. The corresponding topographic profile analysis (Figure 4C) provides quantitative data, showing thickness variations up to ~150 nm. Cross-sectional profiles further reveal asymmetric slopes: Profile 1 displays a steeper transition, while Profile 2 exhibits a more gradual one, suggesting heterogeneous nanoparticle distribution along the surface.

Altogether, these AFM analyses confirm the successful

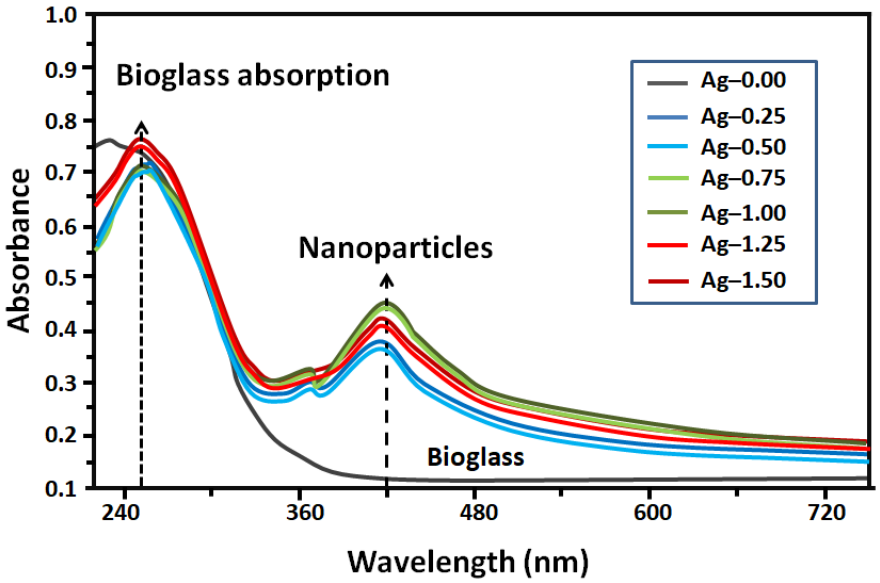

Figure 3. Optical absorption spectra of pure and silver (Ag)-doped nanostructured bioglasses.

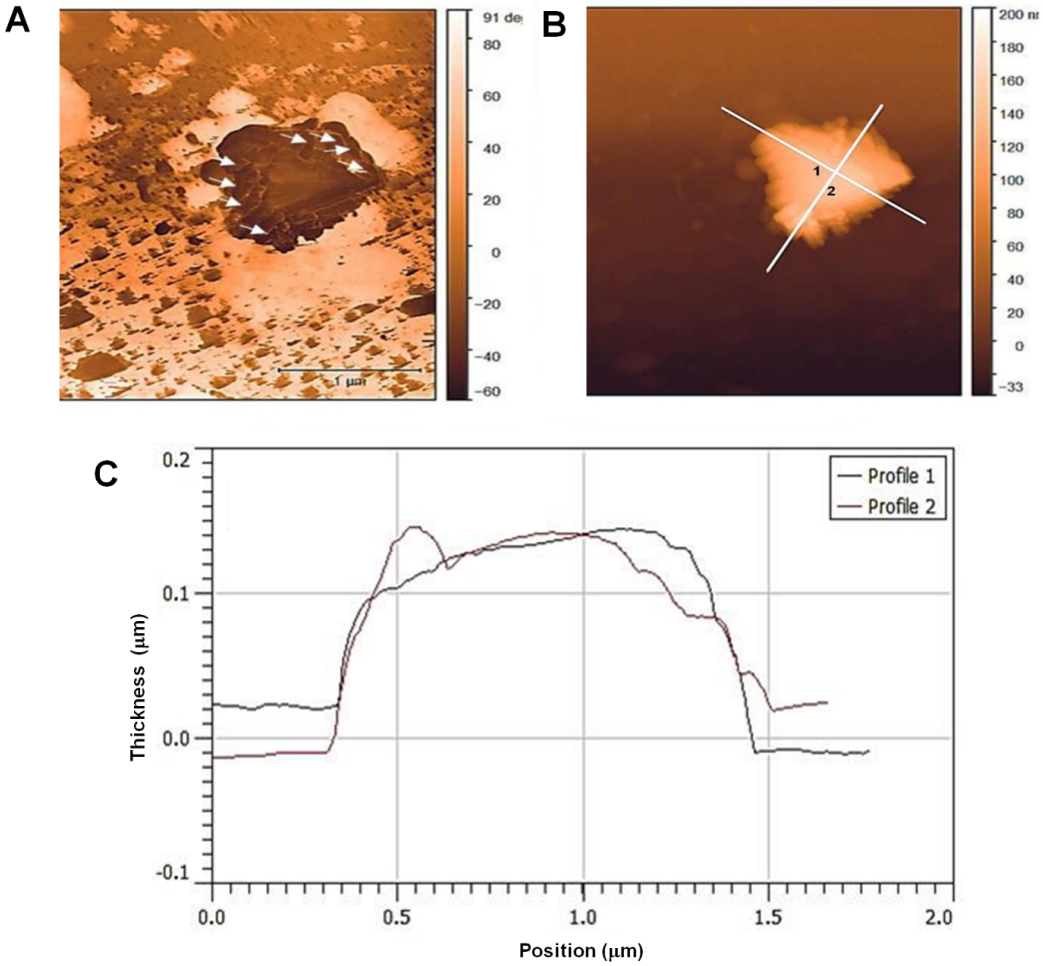

Figure 4. Atomic force microscopy (AFM) phase images of nanostructured bioglasses. (A) White arrows indicate surface heterogeneities associated with nanostructured domains. (B) Representative phase contrast highlighting differences in surface interactions. (C) Phase profile along the selected line, illustrating surface variation across the analyzed region. Scale bar: 1 µm; magnification: 50,000×.

incorporation of AgNPs into the bioglass matrix. The observed morphological and topographical features highlight an overall dispersed pattern with local heterogeneity, which may play a crucial role in enhancing bioactivity, osteointegration, and antimicrobial performance of the nanostructured bioglass.

3.2. Histopathological evaluation

Inter-observer reproducibility for histological scoring was excellent, with a Kappa index of 97.46 ± 4.07%, demonstrating consistency across evaluations.

Residual crystals were absent in the C group, while treated groups exhibited a dose-dependent increase in crystal persistence. Lower Ag concentrations (≤0.50 wt%) showed fewer and more dispersed remnants, whereas groups containing ≥0.75 wt% Ag presented significantly greater crystal retention ($p < 0.001$), which is consistent with the slower dissolution expected for higher dopant levels (Figure 5A-C).

Inflammatory cell infiltration was assessed in two regions: between crystals and at the defect border. In general, treated groups showed mild or absent inflammatory cell infiltration, supporting good local biocompatibility. However, the Ag-0.00 group exhibited marked border inflammation, despite milder scores for the between-crystals region. Among Ag-containing groups, the highest inflammatory scores were observed in Ag-1.00, Ag-1.25, and Ag-1.50, which corresponded with greater crystal retention ($p < 0.001$). In contrast, Ag-0.50 and Ag-0.75 showed the lowest inflammatory levels in both

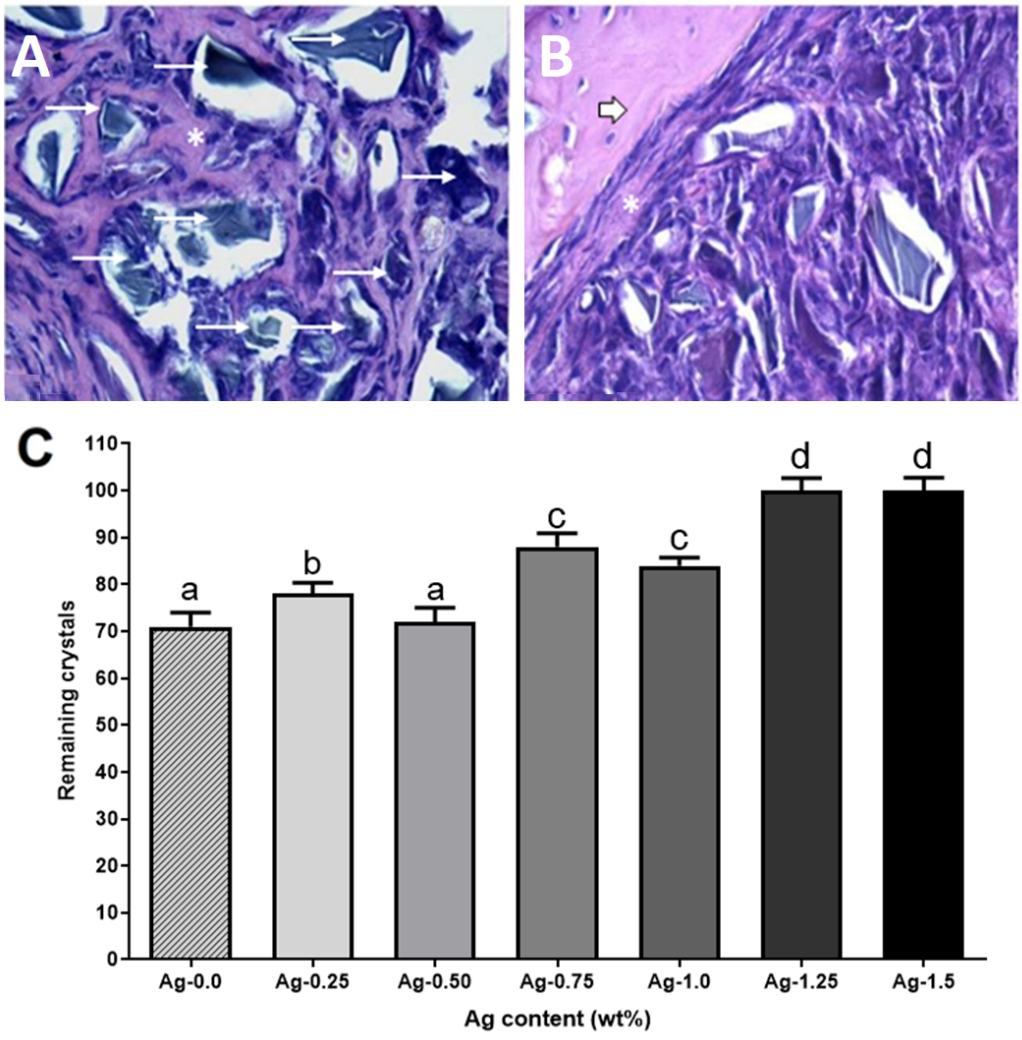

Figure 5. Histological sections of rat calvaria and quantification of residual crystals. (A) Neoformed tissue within the bone defect showing abundant silver crystals (black) surrounded by fibrous connective tissue. Scale bar: 50 µm, magnification: 400×. (B) Bone occupying the defect area, with underlying fibrous connective tissue interspersed among crystals. Scale bar: 50 µm, magnification: 400×. (C) Percentage of samples with moderate to intense (scores 2 + 3) residual crystals. Ag denotes groups implanted with nanostructured bioglasses containing silver at different concentrations; vertical bars represent the proportion of samples with residual crystals. All letters (a, b, c, and d) represent statistically significant differences at the same level of significance ($p < 0.001$), as determined by one-way ANOVA followed by Tukey's multiple comparisons post hoc test.

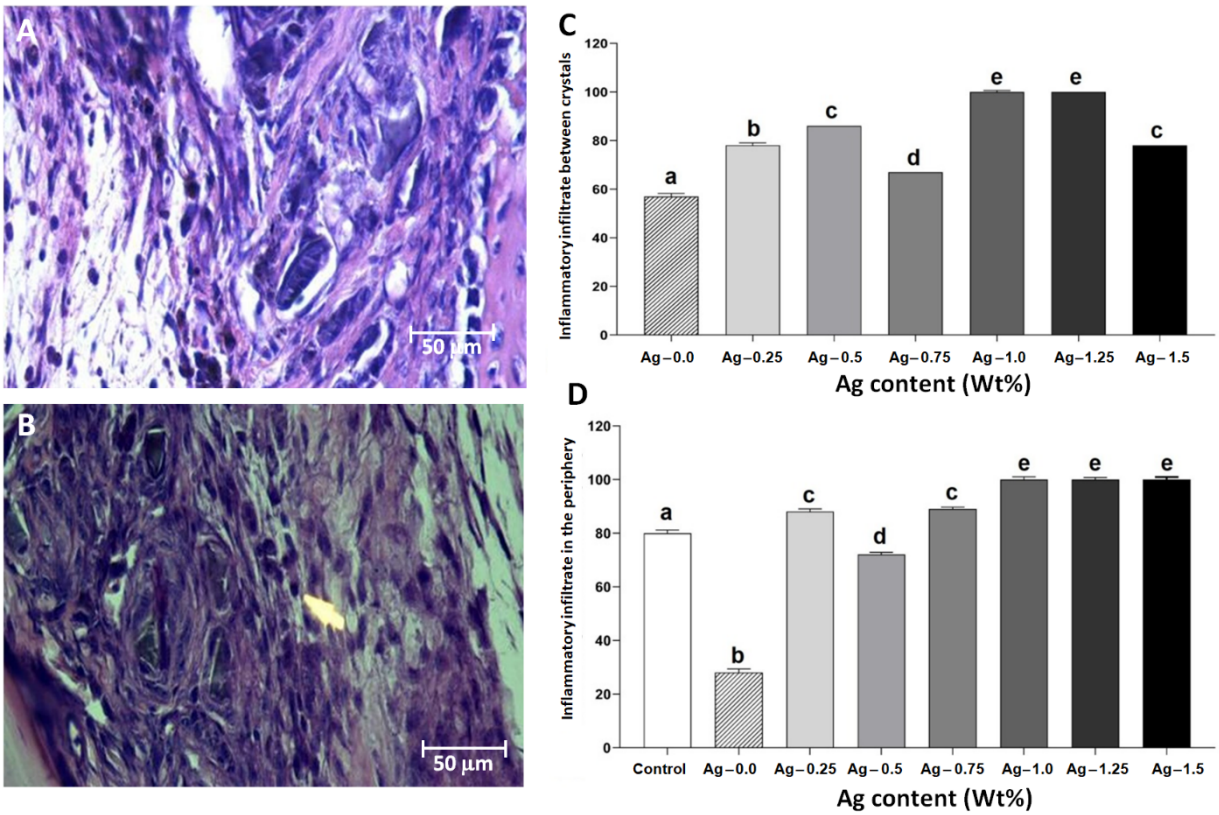

Figure 6. Histological sections and quantification of inflammatory cell infiltration. (A) Region beneath the bone within the defect, showing mild infiltration of mature lymphocytes (arrow) and dispersed crystals. Scale bar: 50 µm, magnification: 400×. (B) Scattered mature lymphocytes (arrow) and crystals located at the periphery of the bone defect. Scale bar: 50 µm, magnification: 400×. (C) Percentage of samples presenting mild or absent inflammatory infiltrates (scores 0 + 1) between crystals. (D) Percentage of samples presenting mild or absent inflammatory infiltrates (scores 0 + 1) at the defect periphery. All letters (a, b, c, and d) represent statistically significant differences at the same level of significance ($p < 0.001$), as determined by one-way ANOVA followed by Tukey's multiple comparisons post hoc test.

regions (Figure 6A-D).

In the C group, the defect was predominantly filled with fibrous/connective tissue, with mild inflammatory infiltrates at the border, consistent with the absence of implanted material. Importantly, no foreign body granulomas, necrosis, abscesses, or multinucleated giant-cell reactions were observed in any group, and the dura mater remained intact.

These findings indicate a clear concentration-dependent pattern. Intermediate Ag levels (0.50–0.75 wt%) were associated with lower inflammation and fewer residual crystals, while higher concentrations led to more persistent material fragments and an increase in inflammatory cell recruitment.

3.3. Systemic histological evaluation

Histological analysis of hepatic and renal tissues was performed to investigate potential systemic effects associated with the implantation of Ag-doped nanostructured bioglasses. Overall, no relevant toxicological alterations were observed in either organ, regardless of Ag concentration.

In the liver, both C and treated groups exhibited predominantly mild histological alterations, including occasional hydropic degeneration, discrete perivascular inflammatory cell infiltration, and minimal vascular congestion. These findings were sporadic and comparable across groups. Hepatocellular necrosis was rare, occurring only in isolated samples, without any apparent association with Ag content. Importantly, no extensive inflammatory foci, fibrotic changes, or granulomatous reactions were detected (Figure 7A).

Renal histological evaluation similarly demonstrated preserved tissue architecture in all experimental groups. The most frequent findings were mild tubular dilation, discrete cytoplasmic vacuolization, and limited vascular congestion, all of which were sporadic and of low severity. Glomerular structures remained intact, with no evidence of sclerosis, mesangial expansion, or inflammatory cell infiltration. No severe renal lesions were observed in any group (Figure 7B).

Semi-quantitative histopathological scoring (Tables 1 and 2) revealed comparable distributions of scores among C and treated groups, confirming the absence of significant

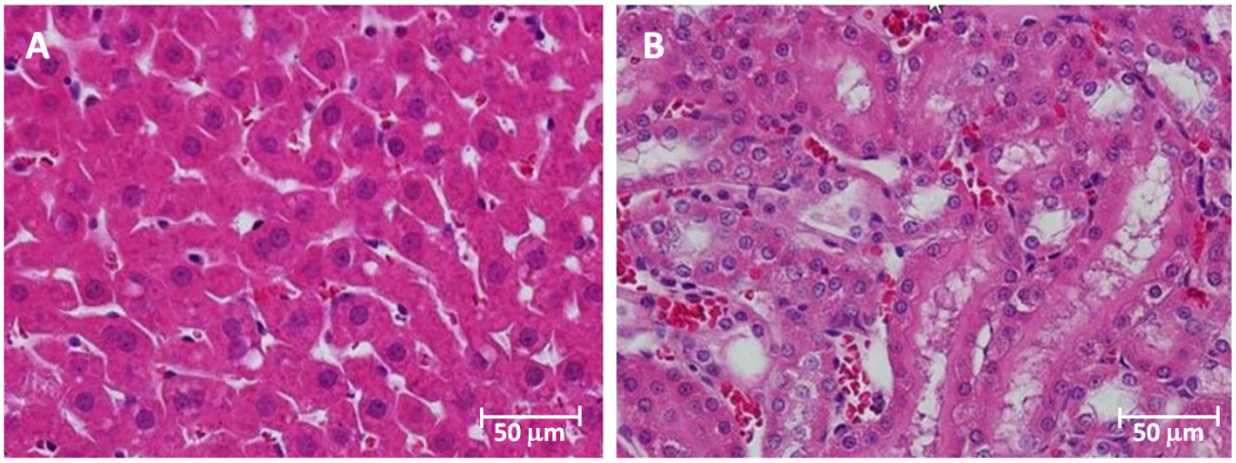

Figure 7. Histological analysis of (A) hepatic and (B) renal tissues of rats after four weeks of bioglass implantation in calvarial bone defects. No significant histopathological alterations were observed in either tissue. Scale bar: 50 µm, magnification: 400×.

hepatotoxic or nephrotoxic effects after four weeks of exposure to nanostructured bioglasses. Representative photomicrographs illustrating the preserved hepatic and renal morphology are presented in Figure 7, corroborating the quantitative and descriptive findings.

Collectively, these results indicate that, within the evaluated experimental period, implantation of Ag-doped nanostructured bioglasses did not induce detectable systemic toxicity in liver or kidney tissues. Nevertheless, the absence of long-term exposure and Ag bioaccumulation analyses is acknowledged and further addressed in the discussion.

3.4. Immunological assessment

Systemic cytokine profiling revealed distinct, concentration-dependent immunomodulatory effects of Ag-doped bioglasses (Figures 8 and 9). Anti-inflammatory cytokines IL-4 and IL-10 were markedly upregulated in specific groups. IL-4 levels were significantly elevated in Ag-0.00 (52.3 ± 4.1 pg/mL) and Ag-1.50 (67.8 ± 5.2 pg/mL) compared with all other Ag-treated groups–Ag-0.25 (38.6 ± 3.9 pg/mL), Ag-0.50 (41.2 ± 4.4 pg/mL), Ag-0.75 (39.5 ± 3.7 pg/mL), Ag-1.00 (42.1 ± 4.0 pg/mL), Ag-1.25 (44.7 ± 4.1 pg/mL)–and the C group (36.8 ± 3.5 pg/mL) (Figure 8A). IL-10 production peaked in Ag-1.50 (73.6 ± 5.8 pg/mL), significantly surpassing all other groups, including Ag-0.00 (48.5 ± 4.5 pg/mL), indicating a strong anti-inflammatory and regulatory response at the highest Ag concentration (Figure 8B).

Pro-inflammatory cytokines exhibited selective modulation across groups. IL-6 levels were highest in Ag-0.00 (61.2 ± 5.1 pg/mL), significantly above all other groups: Ag-0.25 (42.4 ± 4.3 pg/mL), Ag-0.50 (44.1 ± 3.9 pg/mL), Ag-0.75 (45.8 ± 4.0 pg/mL), Ag-1.00 (43.5 ± 4.2 pg/mL), Ag-1.25 (41.9 ± 3.8 pg/mL), Ag-1.50 (40.7 ± 3.5 pg/mL), and C (39.6 ± 3.6 pg/mL) (Figure 9A). TNF-α displayed a biphasic response: Ag-0.25 (56.7 ± 4.9 pg/mL) and Ag-1.00 (58.3 ± 5.2 pg/mL) showed moderate increases, whereas Ag-0.75 (71.5 ± 6.0 pg/mL) induced the highest systemic TNF-α levels, significantly exceeding all groups except Ag-0.50 (63.2 ± 5.4 pg/mL) (Figure 9B). IFN-γ modulation was restricted to Ag-0.25 (35.1 ± 3.7 pg/mL) and Ag-0.75 (52.8 ± 4.6 pg/mL), with the latter significantly higher, suggesting selective T helper cell type 1 activation (Figure 9C).

Collectively, these results suggest that the Ag content of nanostructured bioactive glasses critically shapes systemic immune responses. Very low (Ag-0.00) and very high (Ag-1.50) Ag concentrations favored anti-inflammatory signals, whereas intermediate levels (Ag-0.50–0.75) enhanced pro-inflammatory activity. This dose-dependent immunomodulation may be relevant for balancing inflammation and repair during bone regeneration, reinforcing the biomedical potential of Ag-doped bioactive glasses.

4. Discussion

Biomaterials are increasingly recognized as active modulators of host immune responses, with their biological behavior being strongly influenced by composition, surface chemistry, and structural characteristics. Upon implantation, biomaterials are inevitably identified as foreign entities, triggering inflammatory cascades aimed at isolating, remodeling, or resorbing the material. While inflammation is a necessary component of tissue repair, its magnitude and duration critically shape host responses, particularly in bone repair models, where excessive or prolonged inflammation may alter tissue organization and remodeling dynamics.[18-20] In this context, experimental approaches that can systematically capture immune–inflammatory responses are essential for the biological evaluation of biomaterials.

In the present study, the proposed experimental framework

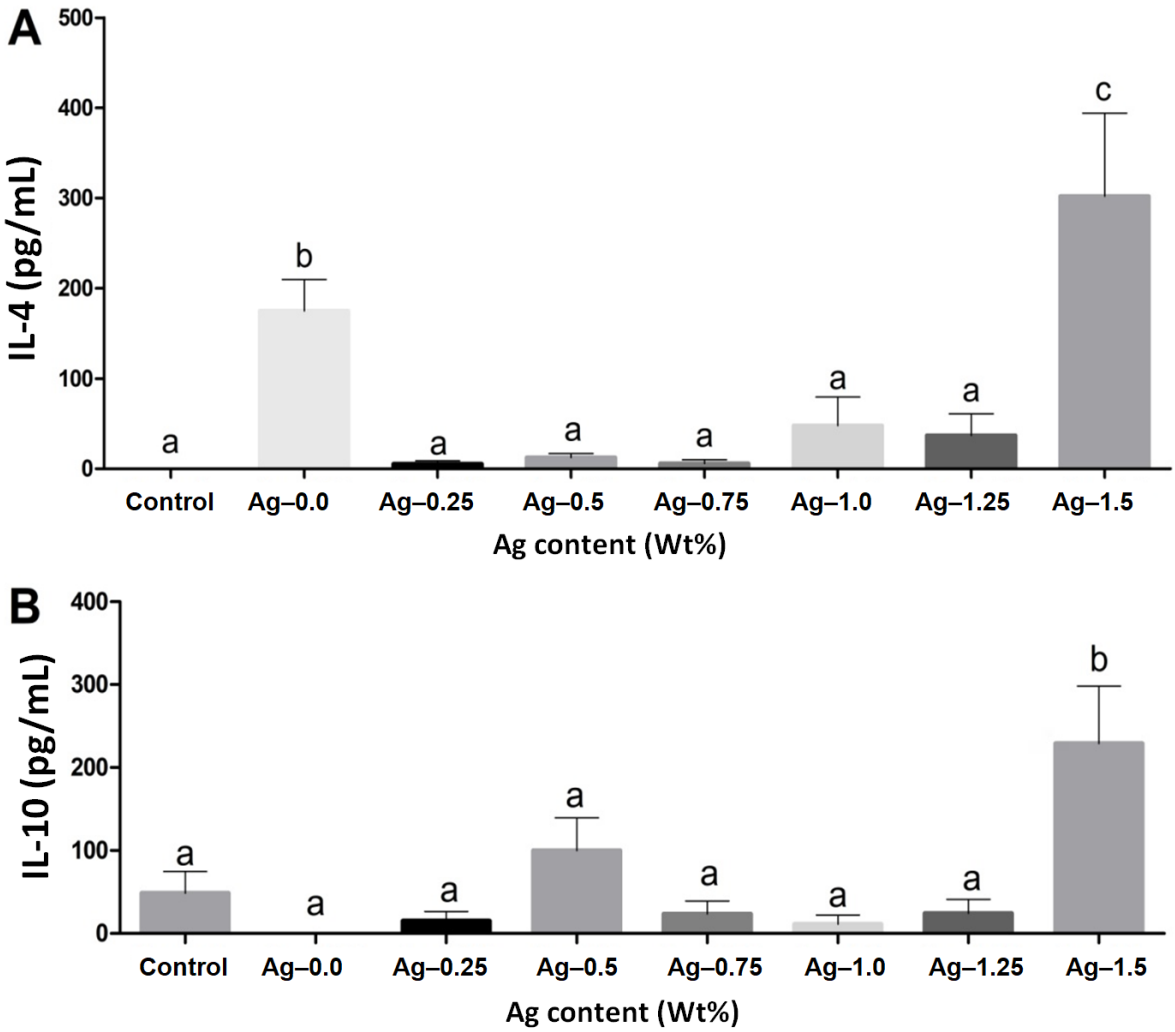

Figure 8. Plasma concentrations of anti-inflammatory cytokines (A) IL-4 and (B) IL-10 in Wistar rats. Values are expressed as mean ± standard error of the mean. Statistical analysis was performed using the Kruskal–Wallis test followed by Dunn's multiple comparisons post hoc test; different letters indicate statistically significant differences ($p < 0.05$).
Abbreviation: IL: Interleukin.

enabled the detection of systemic immune modulation induced by both pure and Ag-doped nanostructured bioglasses. Across formulations, cytokine profiling revealed a shift toward a regulatory immune environment, characterized by increased levels of IL-4 and IL-10. Importantly, Ag incorporation accentuated these effects in a concentration-dependent manner, demonstrating the sensitivity of the methodological approach to resolve dose-related immunological variations. Although macrophage phenotypes were not directly assessed, the observed cytokine profiles are consistent with regulatory immune signaling patterns commonly reported in biomaterial implantation models.[21]

Comparable immune–inflammatory trends have been described in studies evaluating other nanostructured biomaterials, including titanium oxide-based surfaces, in which early inflammatory signaling is followed by sustained production of regulatory cytokines.[22,23] Within this framework, the present findings indicate that the applied methodology is capable of capturing dynamic immune responses associated with material composition and ion incorporation. Nevertheless, mechanistic pathways such as macrophage polarization states, receptor-level activation, or intracellular signaling cascades were not experimentally evaluated and therefore cannot be inferred from the current dataset.

Although macrophage phenotype markers such as CD86 (M1) and CD206 (M2) were not assessed by immunohistochemistry, the cytokine profile evaluated in this study provides functional insights into the immune environment elicited by the biomaterials. Regulatory cytokines IL-4 and IL-10, as well as pro-inflammatory mediators IL-6, TNF-α, and IFN-γ, have been widely employed in preclinical osteoimmunology studies as complementary indicators of immune activation states.[24,25] However, these mediators do not substitute for direct cellular phenotyping, which remains

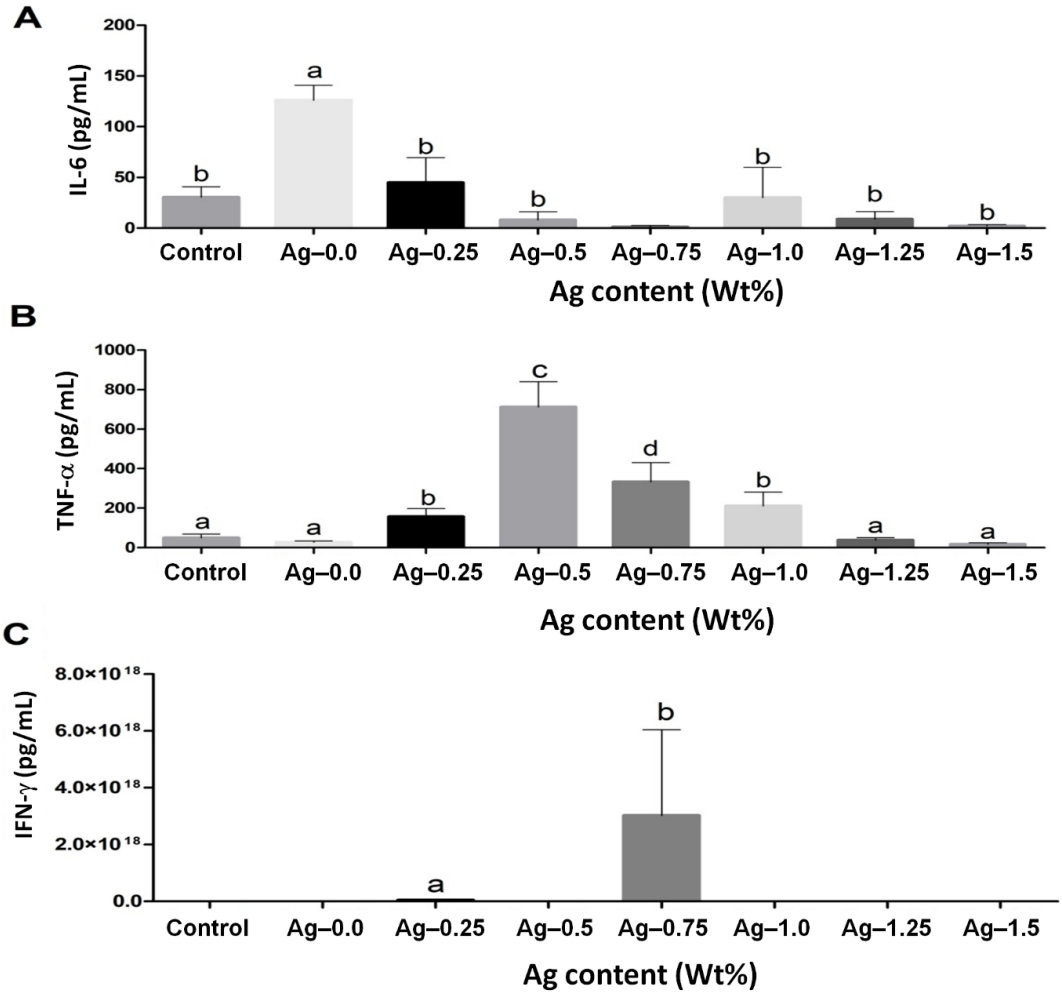

Figure 9. Plasma concentrations of pro-inflammatory cytokines (A) interleukin-6 (IL-6), (B) tumor necrosis factor alpha (TNF-α), and (C) interferon gamma (IFN-γ) in Wistar rats. Values are expressed as mean ± standard error of the mean. Statistical analysis was performed using the Kruskal–Wallis test followed by Dunn's multiple comparisons post hoc test. All letters (a, b, c, and d) represent statistically significant differences at the same level of significance ($p < 0.001$), as determined by one-way ANOVA followed by Tukey's multiple comparisons post hoc test.

essential for mechanistic interpretation.[26]

The modulation of IL-10 observed herein aligns with previous reports describing biomaterial-mediated regulation of immune responses during bone repair.[27,28] IL-10 plays a central role in limiting excessive inflammation and regulating oxidative stress. Consistent with systemic cytokine data, histopathological evaluation of calvarial defects revealed predominantly mild inflammatory infiltrates across treated groups, with preserved tissue architecture and absence of foreign body granulomatous reactions. This correspondence supports the internal consistency of the methodological approach in linking systemic immune markers with local tissue responses, without implying direct causal mechanisms.

Pro-inflammatory cytokines exhibited distinct concentration-dependent patterns. IL-6 levels were more pronounced in the pure bioglass group, whereas Ag incorporation was associated with a reduction in its expression. While transient IL-6 signaling is a known component of early inflammatory responses following biomaterial implantation, sustained elevation has been associated with altered tissue remodeling.[29] TNF-α and IFN-γ levels also varied according to Ag content, further illustrating the capacity of the experimental design to detect nuanced immunological changes across material formulations.[20,30-33] These findings underscore the importance of modulating inflammation in a controlled manner rather than completely suppressing it.

Histopathological analysis additionally revealed the presence of residual bioglass particles, particularly in groups with higher Ag concentrations, without evidence of excessive inflammatory infiltrates or foreign body reactions. These observations indicate that material persistence alone does not necessarily correlate with adverse immune outcomes, highlighting the relevance of integrating histological evaluation with immune profiling when assessing biomaterial–host interactions.[34-36]

Systemic safety represents a critical consideration in studies involving Ag-containing materials. Histological evaluation of hepatic and renal tissues demonstrated only mild and sporadic alterations, with no significant differences between the C and treated groups at the four-week time point. Although these findings support short-term biocompatibility, the experimental framework was not designed to assess long-term Ag accumulation or chronic systemic effects, which remain important topics for future methodological refinement.[37-39]

From a methodological standpoint, several limitations of the present study should be acknowledged. Immune–inflammatory responses were primarily evaluated through systemic cytokine profiling, without direct immunohistochemical characterization of immune cell subsets, such as macrophage phenotypes. Analyses were conducted at a single experimental time point, which limited the assessment of both early and late dynamic immune responses following biomaterial implantation. Although histopathological evaluation provided qualitative information on local inflammatory patterns, tissue organization, and material persistence, quantitative analyses of immune cell populations, molecular signaling pathways, and new bone formation were not performed; therefore, no claims regarding the extent of bone regeneration are made. In addition, tissue Ag accumulation was not quantitatively assessed. While histological evaluation of liver, kidney, and local defect tissues did not reveal overt structural damage or severe inflammatory alterations, analytical quantification of Ag biodistribution and long-term systemic exposure was not conducted. These limitations define important directions for future investigations aimed at expanding and refining the immune-focused methodological framework described in this study.

From a materials characterization perspective, the amorphous structure identified by X-ray diffraction is characteristic of bioactive glasses and is associated with controlled ion release and surface reactivity.[40,41] Ultraviolet–visible spectral features consistent with Ag incorporation further confirmed the successful integration of the dopant within the glass matrix and its concentration dependence.[42,43] In addition, nanoscale surface features identified by AFM are relevant methodological parameters, as nanotopography influences protein adsorption and cell–material interactions.

Collectively, the present study demonstrates that the proposed experimental framework enables reproducible, dose-resolved assessment of systemic and local immune–inflammatory responses elicited by Ag-doped nanostructured bioglasses. While the findings support the applicability of this approach for biomaterial evaluation, the study does not address specific immune cell phenotypes, intracellular signaling pathways, antimicrobial activity, or long-term outcomes. These limitations define important directions for future methodological developments aimed at refining immune-focused strategies for biomaterial assessment.

5. Conclusion

Silver-doped nanostructured bioglasses elicited dose-dependent modulation of immune–inflammatory responses in a rat calvarial defect model, as reflected by systemic cytokine profiles. Variations in Ag content were associated with changes in regulatory cytokines, such as IL-4 and IL-10, and pro-inflammatory mediators, including IL-6, TNF-α, and IFN-γ, highlighting the sensitivity of the proposed framework to detect immune-related differences among material formulations. Histopathological evaluation indicated the absence of overt local or systemic toxicity at the evaluated time point, supporting the short-term biocompatibility of the tested materials. Further studies incorporating quantitative bone assessment, immune cell phenotyping, and long-term evaluation are required to expand the translational relevance of these findings.

Acknowledgments

The authors acknowledge the financial and institutional support from the Minas Gerais Research Foundation (FAPEMIG), the National Council for Scientific and Technological Development (CNPq), the Coordination for the Improvement of Higher Education Personnel (CAPES), and Uberaba's Teaching and Research Foundation (FUNEPU).

Funding

This study was supported by the Minas Gerais Research Foundation (FAPEMIG) under grants RED-00224-23 (Minas Gerais Network of Translational Nanobioplatforms) and RED-APQ-03655-23 (MultiLab).

Conflict of interest

The authors declare that they have no competing interests.

Author contributions

Conceptualization: Gustavo Henrique Marques Ribeiro, Rafael Obata Trevisan, Rodrigo César Rosa

Formal analysis: Renata Margarida Etchebehere, Noelio Oliveira Dantas

Funding acquisition: Rodrigo César Rosa and Carlo José Freire Oliveira

Investigation: Gustavo Henrique Marques Ribeiro, Rafael Obata Trevisan, Malu Mateus Santo Obata, Chamberttan S. Desidério, Carlo José Freire Oliveira, Hugo F. Perini, Marcos Vinicius da Silva

Methodology: Malu Mateus Santo Obata, Chamberttan S. Desidério, Odival Seabra
Resources: Anielle Christine Almeida Silva, Sanívia Aparecida de Lima Pereira
Supervision: Rodrigo César Rosa
Writing–original draft: Gustavo Henrique Marques Ribeiro, Rafael Obata Trevisan
Writing–review & editing: Rodrigo César Rosa, Hugo F. Perini, Carlo José Freire Oliveira

Ethics approval and consent to participate

All animal procedures were conducted in accordance with the Guide for the Care and Use of Laboratory Animals (National Institutes of Health) and were approved by the Institutional Animal Care and Use Committee (CEUA/UNIUBE, protocol no. 004/2021). The committee specifically approved the surgical creation of critical-size calvarial bone defects, postoperative care, and euthanasia procedures, ensuring compliance with ethical standards for animal welfare.

Consent for publication

Not applicable.

Data availability statement

The datasets generated and analyzed during the current study are available from the corresponding author on reasonable request.

References

1. Ambrosio L, Raucci MG, Vadala G, Ambrosio L, Papalia R, Denaro V. Innovative Biomaterials for the Treatment of Bone Cancer. *Int J Mol Sci.* 2021;22(15):8214 doi: 10.3390/ijms22158214.
2. Kopec M, Beton K, Jarczewska K, Abramczyk H**.** Hyperglycemia and cancer in human lung carcinoma by means of Raman spectroscopy and imaging. *Sci Rep.* 2022;12(1):18561. doi: 10.1038/s41598-022-21483-y
3. Marin E, Boschetto F, Pezzotti G. Biomaterials and biocompatibility: An historical overview. *J Biomed Mater Res A.* 2020;108(8):1617-1633. doi: 10.1002/jbm.a.36930
4. Moldovan F, Ivanescu AD, Fodor P, Moldovan L, Bataga T. Correlation between Inflammatory Systemic Biomarkers and Surgical Trauma in Elderly Patients with Hip Fractures. *J Clin Med.* 2023;12(15):5147. doi: 10.3390/jcm12155147
5. Feroz S, Cathro P, Ivanovski S, Muhammad N. Biomimetic bone grafts and substitutes: A review of recent advancements and applications. *Biomed Eng Adv.* 2023;6:100107. doi: 10.1016/j.bea.2023.100107
6. Huang EE, Zhang N, Shen H, *et al*. Novel Techniques and Future Perspective for Investigating Critical-Size Bone Defects. *Bioengineering (Basel).* 2022;9(4):171. doi: 10.3390/bioengineering9040171
7. Quek J, Vizetto-Duarte C, Teoh SH, Choo Y. Towards Stem Cell Therapy for Critical-Sized Segmental Bone Defects: Current Trends and Challenges on the Path to Clinical Translation. *J Funct Biomater.* 2024;15(6):145. doi: 10.3390/jfb15060145
8. Zhu Y, Zhang X, Chang G, Deng S, Chan HF. Bioactive Glass in Tissue Regeneration: Unveiling Recent Advances in Regenerative Strategies and Applications. *Adv Mater.* 2025;37(2):e2312964. doi: 10.1002/adma.202312964
9. Szczesny G, Kopec M, Politis DJ, Kowalewski ZL, Lazarski A, Szolc T. A Review on Biomaterials for Orthopaedic Surgery and Traumatology: From Past to Present. *Materials (Basel).* 2022;15(10):3622. doi: 10.3390/ma15103622
10. Kim SH, Seo YB, Yeon YK, *et al*. 4D-bioprinted silk hydrogels for tissue engineering. *Biomaterials.* 2020;260:120281. doi: 10.1016/j.biomaterials.2020.120281
11. Arron JR, Choi Y. Bone versus immune system. *Nature.* 2000;408(6812):535–536. doi: 10.1038/35046196
12. Minardi S, Taraballi F, Pandolfi L, Tasciotti E. Patterning Biomaterials for the Spatiotemporal Delivery of Bioactive Molecules. *Front Bioeng Biotechnol.* 2016;4:45. doi: 10.3389/fbioe.2016.00045
13. Okamoto K. Crosstalk between bone and the immune system. *J Bone Miner Metab.* 2024;42(4):470–480. doi: 10.1007/s00774-024-01539-x
14. Tu Z, Zhong Y, Hu H, *et al*. Design of therapeutic biomaterials to control inflammation. *Nat Rev Mater.* 2022;7(7):557–574. doi: 10.1038/s41578-022-00426-z
15. Wei X, Lei L, Luo L, Zhou Y, Zheng Z, Chen W. Advances in osteoimmunomodulation of biomaterials after intrabone implantation: focus on surface hydrophilicity. *J Mater Chem B.* 2024;12(43):11089–11104. doi: 10.1039/d4tb01907e
16. Xue Y, Che J, Ji X, Li Y, Xie J, Chen X. Recent advances in biomaterial-boosted adoptive cell therapy. *Chem Soc Rev*. 2022;51(5):1766-1794. doi: 10.1039/d1cs00786f
17. Finger Stadler A, Musskopf ML, Gohel V, *et al*. Evaluation of Two Alloplastic Biomaterials in a Critical-Size Rat Calvarial Defect Model. *J Funct Biomater.* 2025;16(6):214. doi: 10.3390/jfb16060214
18. Guo R, Wang R, Zhang W, *et al*. Macrophage Polarisation in the Tumour Microenvironment: Recent Research Advances and Therapeutic Potential of Different Macrophage Reprogramming. *Cancer Control.* 2025;32:10732748251316604. doi: 10.1177/10732748251316604
19. Yang B, Rutkowski N, Elisseeff J. The foreign body response: emerging cell types and considerations for targeted therapeutics. *Biomater Sci.* 2023;11(24):7730–7747. doi: 10.1039/d3bm00629h
20. Yoshinaga M, Takeuchi O. Regulation of inflammatory

diseases via the control of mRNA decay. *Inflamm Regen.* 2024;44(1):14.
doi: 10.1186/s41232-024-00326-5

21. Gao L, Li M, Yin L, *et al*. Dual-inflammatory cytokines on TiO_2 nanotube-coated surfaces used for regulating macrophage polarization in bone implants. *J Biomed Mater Res A.* 2018;106(7):1878–1886.
doi: 10.1002/jbm.a.36391
22. Mariani E, Lisignoli G, Borzi RM, Pulsatelli L. Biomaterials: Foreign Bodies or Tuners for the Immune Response? *Int J Mol Sci.* 2019;20(3):636.
doi: 10.3390/ijms20030636
23. Yan X, Shen K, Tang Q, *et al*. IL-4 functionalized titanium dioxide nanotubes modulate the inflammatory response of macrophages. *J Biomater Sci Polym Ed.* 2020;31(17):2238–2251.
doi: 10.1080/09205063.2020.1799534
24. Loo YM, Gale M Jr. Immune signaling by RIG-I-like receptors. *Immunity.* 2011;34(5):680–692.
doi: 10.1016/j.immuni.2011.05.003
25. Medina MA, Fuentes-Villalobos F, Quevedo C, *et al*. Longitudinal transcriptional changes reveal genes from the natural killer cell-mediated cytotoxicity pathway as critical players underlying COVID-19 progression. *Elife.* 2024;13:RP94242.
doi: 10.7554/eLife.94242
26. Zhang D, Jiang L, Li L, *et al*. Integrated metabolomics revealed the fibromyalgia-alleviation effect of Mo_2C nanozyme through regulated homeostasis of oxidative stress and energy metabolism. *Biomaterials.* 2022;287:121678.
doi: 10.1016/j.biomaterials.2022.121678
27. Hotchkiss KM, Reddy GB, Hyzy SL, Schwartz Z, Boyan BD, Olivares-Navarrete R. Titanium surface characteristics, including topography and wettability, alter macrophage activation. *Acta Biomater.* 2016;31:425–434.
doi: 10.1016/j.actbio.2015.12.003
28. Laquerriere P, Grandjean-Laquerriere A, Jallot E, *et al*. Influence of the zinc concentration of sol-gel derived zinc substituted hydroxyapatite on cytokine production by human monocytes in vitro. *Biomaterials*. 2006;27(17):3195-200.
doi: 10.1016/j.biomaterials.2006.01.024
29. Condorelli M, Speciale A, Cimino F, *et al*. Nano-Hybrid Au@LCCs Systems Displaying Anti-Inflammatory Activity. *Materials (Basel).* 2022;15(10):3701.
doi: 10.3390/ma15103701
30. Amani H, Alipour M, Shahriari E, Taboas JM. Immunomodulatory Biomaterials: Tailoring Surface Properties to Mitigate Foreign Body Reaction and Enhance Tissue Regeneration. *Adv Healthc Mater*. 2024;13(29):e2401253.
doi: 10.1002/adhm.202401253
31. Lee HS, Stachelek SJ, Tomczyk N, Finley MJ, Composto RJ, Eckmann DM. Correlating macrophage morphology and cytokine production resulting from biomaterial contact. *J Biomed Mater Res A.* 2013;101(1):203–212.
doi: 10.1002/jbm.a.34309
32. Pandey S, Bednarz P, Veiseh O. Tuning Biomaterial Surfaces to Modulate Host-Immune Reactions. *Langmuir.* 2025;41(27):17355–17368.
doi: 10.1021/acs.langmuir.5c01344
33. Yu W, Fu L, Lei G, *et al*. Chemokine Ligands and Receptors Regulate Macrophage Polarization in Atherosclerosis: A Comprehensive Database Mining Study. *CJC Open.* 2024;7(3):310–324.
doi: 10.1016/j.cjco.2024.11.018
34. Bi Z, Cai Y, Shi X, *et al*. Macrophage-mediated immunomodulation in biomaterial-assisted bone repair: Molecular insights and therapeutic prospects. *Chem Eng J.* 2024;488:150631.
doi: 10.1016/j.cej.2024.150631
35. Kajander K, Nowak N, Vaziri N, Vallittu PK, Heino TJ, Maatta JA. Unraveling the immunomodulatory and metabolic effects of bioactive glass S53P4 on macrophages in vitro. *J Mater Sci Mater Med.* 2025;36(1):13.
doi: 10.1007/s10856-025-06861-y
36. Pajares-Chamorro N, Wagley Y, Maduka CV, *et al*. Silver-doped bioactive glass particles for in vivo bone tissue regeneration and enhanced methicillin-resistant *Staphylococcus aureus* (MRSA) inhibition. *Mater Sci Eng C Mater Biol Appl.* 2021;120:111693.
doi: 10.1016/j.msec.2020.111693
37. Furko M. Bioglasses Versus Bioactive Calcium Phosphate Derivatives as Advanced Ceramics in Tissue Engineering: Comparative and Comprehensive Study, Current Trends, and Innovative Solutions. *J Funct Biomater.* 2025;16(5):161. doi: 10.3390/jfb16050161
38. Nosrati H, Hamzepoor M, Sohrabi M, *et al*. The potential renal toxicity of silver nanoparticles after repeated oral exposure and its underlying mechanisms. *BMC Nephrol.* 2021;22(1):228.
doi: 10.1186/s12882-021-02428-5
39. Shirgill S, Poologasundarampillai G, Jabbari S, Ward J, Kuehne SA. Silver-doped bioactive glass fibres as a potential treatment for wound-associated bacterial biofilms. *Bio ilm.* 2023;5:100115.
doi: 10.1016/j.bioflm.2023.100115
40. Mcoyi M, Mpofu K, Sekhwama M, Mthunzi-Kufa P. Developments in Localized Surface Plasmon Resonance. *Plasmonics.* 2024;20:5481–5520.
doi: 10.1007/s11468-024-02620-x
41. Mirt AL, Ficai D, Oprea OC, Vasilievici G, Ficai A**.** Current and Future Perspectives of Bioactive Glasses as Injectable Material. *Nanomaterials (Basel).* 2024;14(14):1196.
doi: 10.3390/nano14141196
42. Alzoubi FY, Ahmad AA, Aljarrah IA, *et al*. Localize surface plasmon resonance of silver nanoparticles using Mie theory. *J Mater Sci Mater Electron.* 2023;34:2128
doi: 10.1007/s10854-023-11304-x
43. Luo J, Walker M, Xiao Y, Donnelly H, Dalby MJ, Salmeron-Sanchez M. The influence of nanotopography on cell behaviour through interactions with the extracellular matrix–A review. *Bioact Mater.* 2022;15:145–159.
doi: 10.1016/j.bioactmat.2021.11.024